J Solid State Electrochem (2015) 19:967–974
DOI 10.1007/s10008-014-2702-x

ORIGINAL PAPER

Preparation of nanoporous Ag@TiO_2 ribbons through dealloying and their electrocatalytic properties

Guijing Li · Xiaolong Zhang · Xiaoping Song · Zhanbo Sun · Wenjie Feng

Received: 7 July 2014 / Revised: 1 December 2014 / Accepted: 4 December 2014 / Published online: 18 December 2014

Abstract Nanoporous Ag@TiO_2 composites with core-shell structure were successfully prepared through dealloying the melt-spun Al-Ag-Ti ribbons in NaOH aqueous solution. The results revealed that TiO_2 shell with thickness of about 2 nm was formed in situ on the Ag ligaments. Ti^{3+} and Ag^{+} species co-existed after the dealloyed samples were calcined at 873 K, which had significant influence on the catalytic performance. The electrochemical results showed that the nanoporous Ag@TiO_2 composites significantly promoted the direct oxidation of BH_4^- superior to pure Ag. The enhanced catalytic activity could be attributed to the strong interfacial effects between the ligaments and TiO_2 shells.

Keywords Silver · Dealloying · Titanium dioxide · Borohydride oxidation

Introduction

Recently, unsupported nanoporous noble metals prepared by dealloying, such as Au, Pd, and Ag, have attracted great attention in the field of catalysis due to their high specific area, low density, and high electrical conductivity [1–5]. For example, nanoporous Au could exhibit remarkably high catalytic oxidation for methanol and carbon monoxide [6, 7]. Dealloying is one more effective and controllable approach to prepare nanoporous metals and alloys, which essentially involves the selective dissolution of active elements and the rearrangement of inert elements [8, 9]. Though nanoporous metals prepared by dealloying have a more stable structure in comparison with nanoparticles, they are also easy to coarsen at far below the melting temperature, resulting in the degradation of catalytic performances [10].

To functionalize the inner surfaces, many researchers have attempted to load oxides, such as TiO_2 and Al_2O_3, inside the nanoporous metals by impregnation or deposition methods [11–13]. The activity, catalytic selectivity, and stability of nanoporous metals are significantly improved by the strong interfacial effects between metals and oxides. Lang et al. [14] developed a nanoporous gold/MnO_2 electrode by the combination of dealloying and plating. The nanoporous metal/oxide hybrid electrode shows high specific capacitances and charge/discharge rates due to the enhanced conductivity. Nevertheless, the precursors of oxides are usually gathering on the surfaces during deposition process because of the high-aspect ratio of nanoporous structures [13, 15].

Compared with other noble metals, silver is an attractive noble metal for industrial applications owing to its higher electrical conductivity and lower cost. Therefore, the preparation and structure control of nanoporous Ag have been investigated more extensively by dealloying different precursor alloys in recent years [5, 16–18]. However, the catalytic performance of nanoporous Ag should be further enhanced. Nanosized TiO_2 with chemical stability and high activity is one of the most promising catalyst materials. In order to modify the optical and photoelectrochemical properties of Ag, Ag/TiO_2 nanostructures, especially the Ag core and TiO_2 shell structure, have been developed by sol–gel or wet chemical methods [19–22]. It has been found that Ag/TiO_2 nanocomposites could exhibit the enhanced thermostability and optical properties because of the interfacial effects between Ag and TiO_2. Therefore, Ag/TiO_2 composites show

G. Li · X. Zhang · X. Song · Z. Sun (✉)
School of Science, Key Laboratory of Shaanxi for Advanced Functional Materials and Mesoscopic Physics, State Key Laboratory for Mechanical Behavior of Materials, Xi'an Jiaotong University, Xi'an 710049, People's Republic of China
e-mail: szb@mail.xjtu.edu.cn

G. Li · W. Feng
Department of Engineering Mechanics, Shijiazhuang Tiedao University, Shijiazhuang 050043, People's Republic of China

potential application in the fields of catalysis, optics, and solar energy. In comparison, less attention has been given to the electrocatalytic characteristics of Ag/TiO_2 composites.

In our previous studies, CeO_2 nanoparticles were successfully formed in situ on the inner surfaces of the nanoporous Ag and Ag-Au alloys by simply dealloying in a NaOH solution and calcining in air [23, 24]. In this study, we were devoted to investigating the formation of TiO_2 film on the inner surfaces of nanoporous Ag by dealloying the melt-spun Al-Ag-Ti ribbons. Moreover, the electrocatalytic activity of the $Ag@TiO_2$ catalysts for the electrooxidation of borohydride was also investigated. The microstructure and interfacial characteristics of the nanoporous composites were further studied.

Experimental

The preparation of the Al-Ag-Ti precursor alloys was described in our previous work [23]. $Al_{80-X}Ag_{20}Ti_X$ (X=0.5, 1, 2, 3) alloys with nominal composition were prepared by an arc-melting in high-purity Ar atmosphere. The mixture of pure Al (99.90 %), pure Ag (99.99 %), and pure Ti (99.90 %) in a water-cooled copper crucible was melted by arc using a nonconsumable tungsten electrode. Several times of remelting were performed with the ingot turned upside down. The broken ingot inserted into a quartz tube was heated by high frequency induction, and the melt-spun ribbons were achieved after the metal solution was blown onto the surface of a pure Cu roller melt spinning at a speed of 33 ms^{-1}.

The melt-spun Al-Ag-Ti precursor ribbons were dealloyed in a 10 wt.% NaOH aqueous solution until no obvious bubbles emerged (room temperature: 298 K). The phase structures of the ribbons before and after dealloying were analyzed by a Bruker D8 advanced X-ray diffraction (XRD). The dealloyed ribbons were calcined in a muffle furnace at 873 K for 1 h. In order to determine the existence and valence states of Ag and Ti, X-ray photoelectron spectra (XPS) measurements were carried out on a K-Alpha spectrometer (Thermo Electron, USA) using Al Kα X-ray source (1486.68 eV). The spot and energy step size were 400 μm and 0.100 eV, respectively. The total acquired time was 50.3 s. The microstructures of the samples were characterized by JSM-7000 F scanning electron microscope (SEM, JEOL Ltd) and JEM-2100 high-resolution transmission electron microscope (HRTEM, JEOL Ltd). The melt-spun Al-Ag-Ti precursor ribbons were dealloyed in a 20 wt.% NaOH aqueous solution at 333 K for 30 h to remove the residual Al, and the dealloyed sample calcined at 873 K in air for 1 h. The phase structures and microstructures of the samples were characterized by XRD, SEM, and TEM, respectively. The Brunauer–Emmett–Teller (BET) surface areas of the dealloyed $Al_{79.5}Ag_{20}Ti_{0.5}$, $Al_{78}Ag_{20}Ti_2$ and $Al_{77}Ag_{20}Ti_3$ after calcination were measured on an ASAP 2020 surface area analyzer. The samples were degassed at 473 K for 6 h.

The electrochemical measurements were performed in a standard three-electrode cell system by a VersaSTAT MC workstation. A glassy carbon rod with a diameter of 3.0 mm was used as the working electrode, and a pure Pt net with an area of 1.0 cm^2 was employed as the counter electrode. A saturated silver chloride electrode (Ag-AgCl Saturated KCl) was used as the reference. The current density was normalized to the geometrical area of the working electrode. The catalyst ink was prepared by mixing 5.0 mg of the as-prepared composite powder, 1.0 mg of acetylene black, 200.0 μl of isopropanol, and 200.0 μl of 0.5 wt.% Nafion solutions. After the mixture was sonicated for 30 min in a plastic centrifuge tube, 4.0 μl catalyst inks were placed on a polished glassy carbon working electrode. Prior to each electrochemical measurement, the electrolyte (0.5 M KOH+20 mM $NaBH_4$) was replaced with fresh solution and deoxygenated by ultrapure N_2 for 30 min. The measurements were conducted at room temperature (298 K) under the protection of ultrapure N_2.

Results and discussion

Figure 1 shows the XRD patterns of the melt-spun $Al_{80-X}Ag_{20}Ti_X$ (X=0.5, 1, 2, 3) ribbons before and after dealloying in a 10 wt.% NaOH solution at room temperature. The $Al_{79.5}Ag_{20}Ti_{0.5}$ and $Al_{79}Ag_{20}Ti_1$ ribbons, as shown in Fig. 1a, were composed of α-Al, Al_2Ti and Ag_2Al compounds. With the increase of Ti content, Al_3Ti compound appeared in the $Al_{78}Ag_{20}Ti_2$ and $Al_{77}Ag_{20}Ti_3$ alloys besides α-Al and Ag_2Al. It was noticed that the relative intensity of Ag_2Al compound peaks became stronger. From Fig. 1b, it could be seen that all the dealloyed Al-Ag-Ti alloys consisted of Ag, Ag_2Al, and Al-Ti compounds. The results confirmed that only α-Al was decomposed completely, and most of Ag_2Al and Al-Ti compounds remained during dealloying.

Figure 2 shows the XPS spectra of Ag 3d and Ti 2p for the dealloyed melt-spun $Al_{79}Ag_{20}Ti_1$ alloy in a 10 wt.% NaOH solution at room temperature before and after calcination at 873 K. The XPS spectra of Ag 3d exhibited doublet peaks at 368.08 and 374.08 eV, as shown in Fig. 2a, suggesting that Ag is mainly present as Ag^0. While, the XPS peaks of Ag shifted to lower binding energy after the dealloyed sample calcination, which could be attributed to the formation of a certain amount of Ag_2O [25, 26]. Figure 2b shows the XPS peaks of Ti 2P located at 458.68 and 464.28 eV. The peaks were attributed to the formation of TiO_2 in the dealloyed Al-Ag-Ti alloys. The peaks at 458.68 and 464.28 eV shifted to lower binding energy by 1.1 and 0.9 eV, respectively, after the dealloyed sample calcination, which indicates that Ti^{4+} and Ti^{3+} species co-exist in the composites [27, 28]. The XPS results demonstrated that TiO_2 was formed by dealloying the

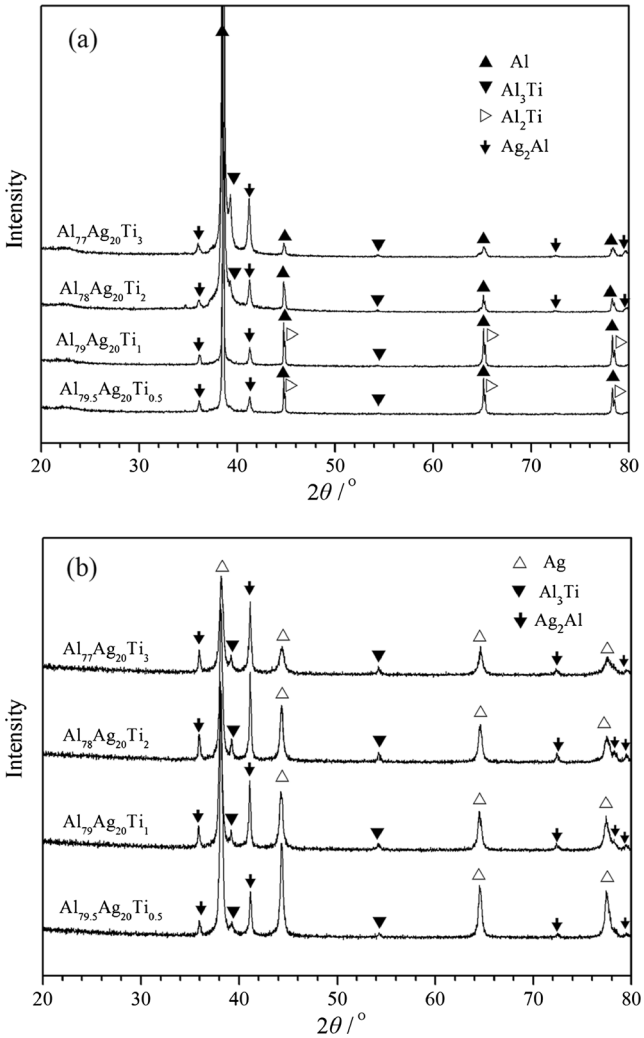

Fig. 1 XRD patterns of the melt-spun Al-Ag-Ti ribbons before (**a**) and after (**b**) dealloying in a 10 wt.% NaOH solution at room temperature

Al-Ag-Ti alloys, and Ag^{+} and Ti^{3+} species were emerged in the composites after calcination in air.

Figure 3 shows the microstructure of the prepared samples by calcining the dealloyed $Al_{80-X}Ag_{20}Ti_X$ (X=0.5, 1, 2, 3) ribbons at 873 K. From Fig. 3a, it can be seen that the surface of the dealloyed $Al_{79.5}Ag_{20}Ti_{0.5}$ ribbons exhibited a porous honeycomb structure, and the polygonal domains were constituted by plate-like ligaments, as denoted by the arrow. According to the results of our previous study, the plate-like ligaments should be the Ag_2Al intermetallic compound [23]. With the increase of Ti content in the precursor alloys, the surface morphology of the dealloyed $Al_{79}Ag_{20}Ti_1$ and $Al_{78}Ag_{20}Ti_2$ ribbons, as shown in Fig. 3b and c, were changed obviously. The plate-like ligaments, as marked by the arrow, became coarsening, and the area of the polygonal domain was distinctly increased. However, the porosity of the dealloyed $Al_{77}Ag_{20}Ti_3$ alloy was significantly decreased, as shown in Fig. 3d. The above results indicate that the content of Ti in the precursory alloys has an important influence on the morphology of the nanoporous $Ag@TiO_2$ composites.

Figure 4 shows the TEM and HRTEM images of the dealloyed $Al_{79}Ag_{20}Ti_1$ ribbons before and after calcination at 873 K. The dealloyed sample, as shown in Fig. 4a, exhibited a typical nanoporous structure with a pore channel size of ~50 nm. The ligaments were interconnected and mutually overlapped. From Fig. 4b, it can be seen that the surface of Ag ligament was covered by a layer of nano film (marked by the arrow). However, the nanoporous structure and the film on the ligaments of the dealloyed samples were not changed obviously after calcination at 873 K, as shown in Fig. 4c and d.

In order to promote the decomposition of Ag_2Al and Ti-Al compounds, the $Al_{80-X}Ag_{20}Ti_X$ (X=1, 2, 3) ribbons were dealloyed in a 20 wt.% NaOH solution at 333 K (water bath heating) for 30 h, and the dealloyed sample calcined at 873 K

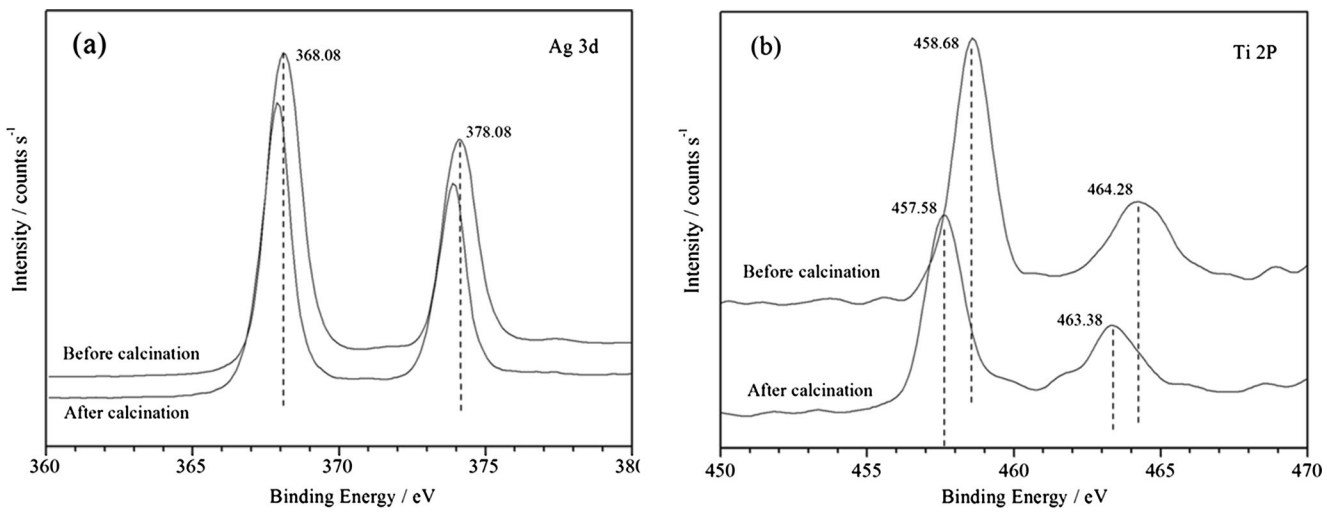

Fig. 2 XPS spectra of Ag 3d (**a**) and Ti 2p (**b**) for the dealloyed melt-spun $Al_{79}Ag_{20}Ti_1$ alloy in a 10 wt.% NaOH solution at room temperature before and after calcination at 873 K in air for 1 h

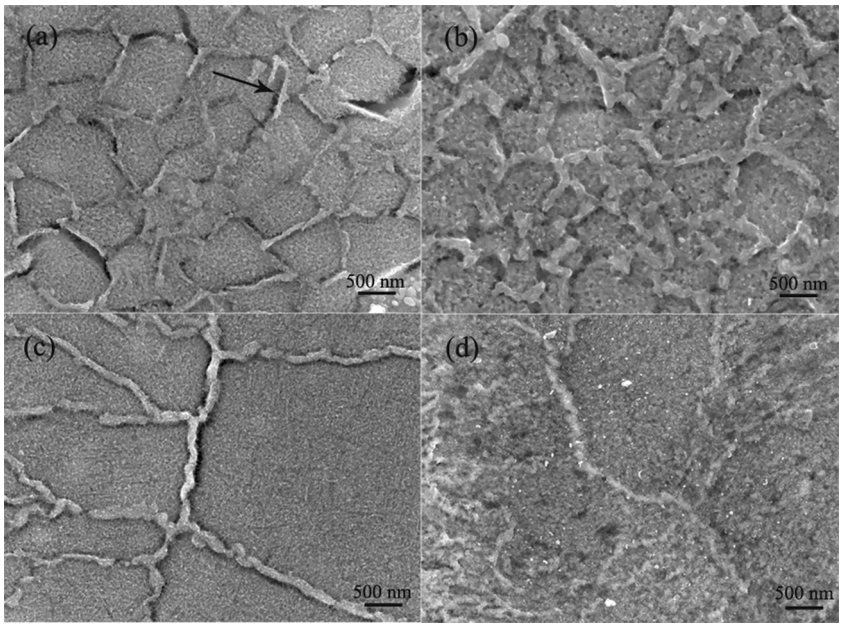

Fig. 3 Plan-view SEM images showing the microstructure of the $Al_{79.5}Ag_{20}Ti_{0.5}$ (**a**), $Al_{79}Ag_{20}Ti_1$ (**b**), $Al_{78}Ag_{20}Ti_2$ (**c**), and $Al_{77}Ag_{20}Ti_3$ (**d**) ribbons dealloyed in a 10 wt.% NaOH solution at room temperature (298 K), the dealloyed sample calcined at 873 K in air for 1 h

in air for 1 h. Figure 5 shows the surface and cross-section microstructure of the prepared samples. The dealloyed $Al_{79}Ag_{20}Ti_1$ ribbons, as shown in Fig. 5a, exhibited a uniform nanoporous structure. The honeycomb structures and plate-like ligaments appeared in Fig. 3b could not be observed. The pore channels with an average size of about 50 nm ran throughout the whole ribbons, as shown in Fig. 5b. With the increase of Ti, though the plate-like ligaments could be observed on the surface of the dealloyed $Al_{78}Ag_{20}Ti_2$ alloy, the porosity, as shown in Fig. 5c, was significantly increased. The cross section of the dealloyed sample, as shown in Fig. 5d, still exhibited an ultrafine porous structure. With the further increase of Ti in the precursor alloy, the porous structure had not been formed in the dealloyed $Al_{77}Ag_{20}Ti_3$, as shown in Fig. 5e and f.

The microstructures of the Al-Ag-Ti ribbons dealloyed at 333 K were further studied in more details by TEM. Figure 6

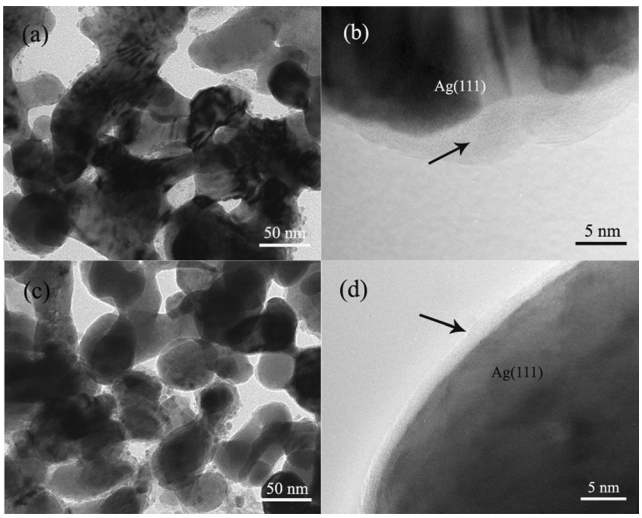

Fig. 4 TEM and HRTEM of the dealloyed melt-spun $Al_{79}Ag_{20}Ti_1$ alloy in a 10 wt.% NaOH solution at room temperature before (**a** and **b**) and after (**c** and **d**) calcination at 873 K in air for 1 h

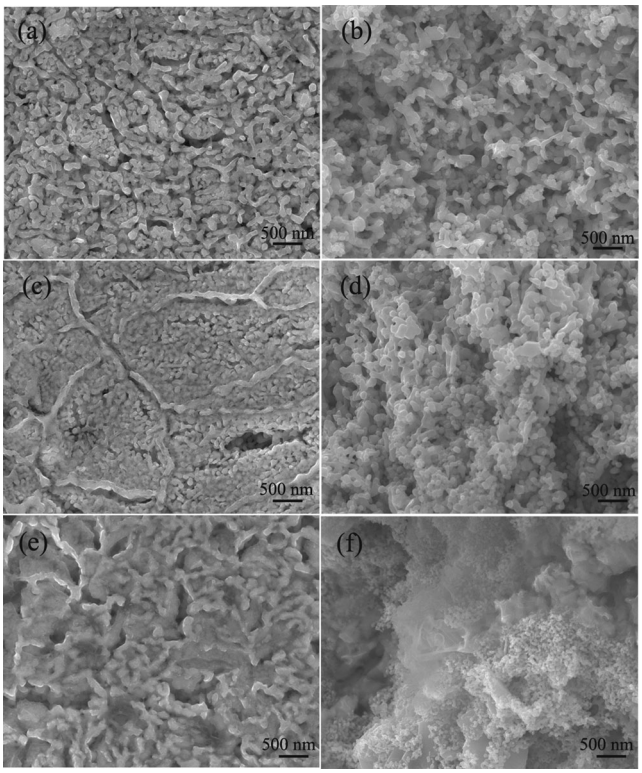

Fig. 5 Plan-view SEM images showing the microstructure of the dealloyed $Al_{79}Ag_{20}Ti_1$ (**a**), $Al_{78}Ag_{20}Ti_2$ (**c**), and $Al_{77}Ag_{20}Ti_3$ (**e**) ribbons in a 20 wt.% NaOH solution at 333 K for 30 h, and the dealloyed sample calcined at 873 K in air for 1 h. Figure 5(**b**), 5(**d**), 5(**f**) showing the corresponding section views

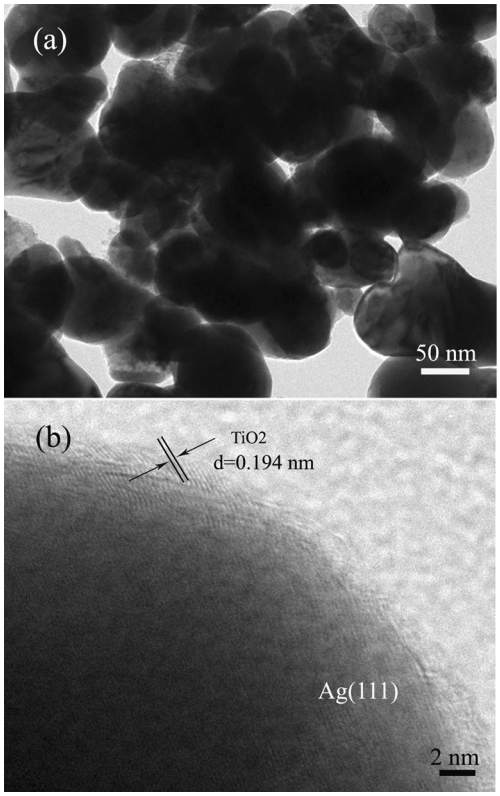

Fig. 6 TEM (**a**) and HRTEM (**b**) images of the dealloyed $Al_{79}Ag_{20}Ti_1$ ribbons in a 20 wt.% NaOH solution at 333 K for 30 h after calcination at 873 K in air

shows the TEM and HRTEM images of the dealloyed $Al_{79}Ag_{20}Ti_1$ ribbons dealloyed in a 20 wt.% NaOH solution at 333 K for 30 h after calcination at 873 K in air. The sample, as shown in Fig. 4a, exhibited a typical nanoporous structure with a pore channel size of ~40 nm. The Ag ligaments with a size of 100 nm were interconnected. The surface of Ag ligament, as shown in Fig. 4b, was wrapped by TiO_2 nano film (the distance of crystal face: 0.194 nm). The results indicated that the nano film observed in Fig. 4b and d was amorphous TiO_2, and its crystallization could be improved by the water bath heating during dealloying.

The phases present were investigated in the Al-Ag-Ti ribbons dealloyed by using water bath heating. Figure 7 shows the XRD patterns of the dealloyed melt-spun $Al_{80-X}Ag_{20}Ti_X$ (X=0.5, 1, 2, 3) ribbons in a 20 wt.% NaOH solution at 333 K for 30 h. The dealloyed samples were calcined at 873 K in air for 1 h. Apparently, all the prepared samples consisted of Ag besides a small quantity of Ag_2Al, and the peaks of Al-Ti compounds observed in Fig. 1b disappeared. The results verify that the Al-Ti and most of Ag_2Al were decomposed. However, TiO_2 in the nanoporous composites was not detected by XRD due to the degree of crystallization.

It is well-known that the dealloying mechanism of Al-Ag alloys is that the active Al is selectively dissolved and the noble Ag atoms are rearranged, which results in the formation of nanoporous Ag [29, 30]. In this report, the melt-spun Al-Ag alloys with a certain amount of Ti were composed of α-Al, Ag_2Al, and Al-Ti compounds (Fig. 1). As the α-Al and Ag_2Al compound were decomposed in NaOH solution, the remaining Ag atoms rearranged and constructed a porous structure. On the other hand, Ti also remained in the porous structure due to its stability in alkali solutions. When the dealloyed samples were exposed to the air, the amorphous TiO_2 films were formed on the Ag ligaments because Ti is more prone to oxidation [31]. As a result, the nanoporous Ag@TiO_2 core-

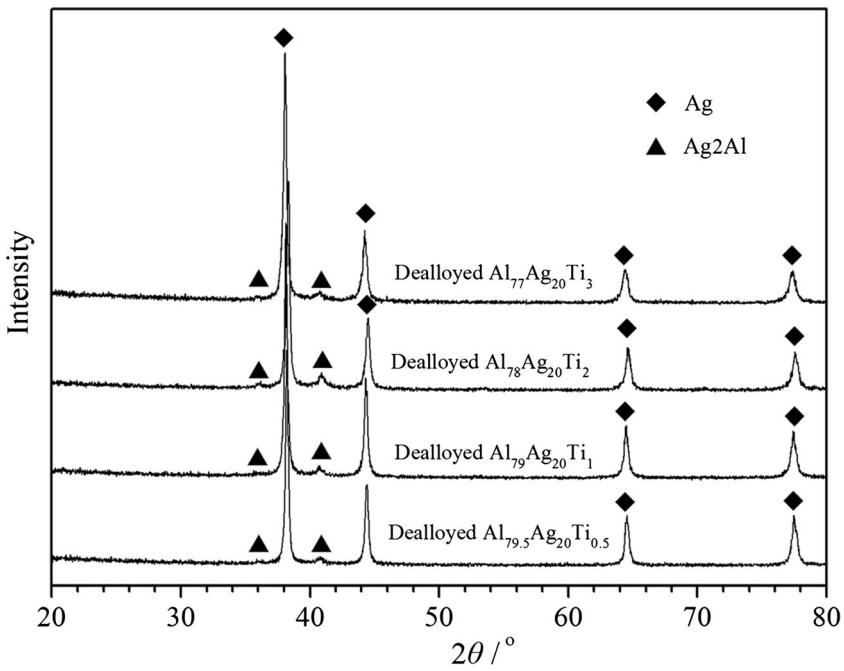

Fig. 7 XRD patterns of the dealloyed melt-spun $Al_{80-X}Ag_{20}Ti_X$ (X=0.5, 1, 2, 3) ribbons in a 20 wt.% NaOH solution at 333 K for 30 h. The dealloyed samples were calcined at 873 K in air for 1 h

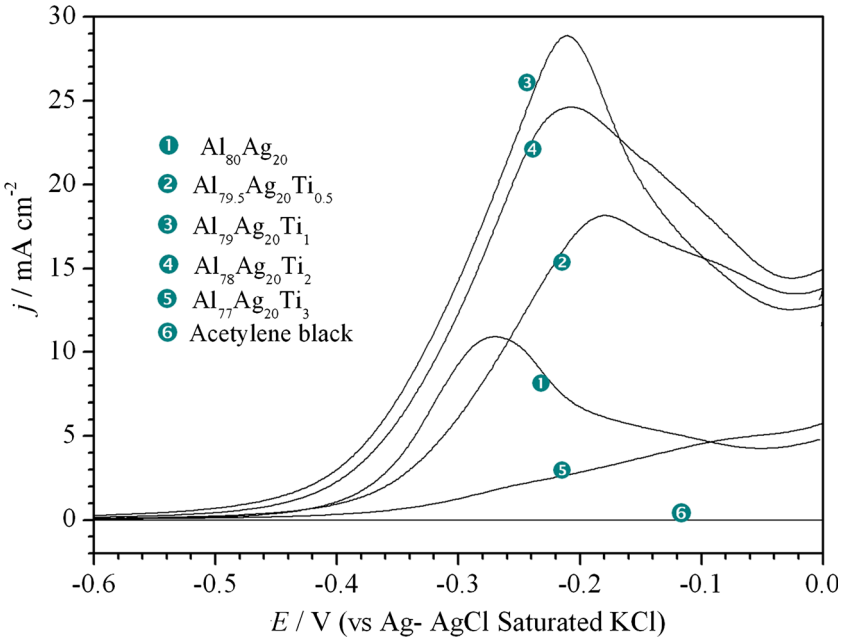

Fig. 8 CV curves of 20 mM $NaBH_4$ in a 0.5 M KOH solution on the nanoporous Ag/TiO_2, Ag, and acetylene black. The scan rate is 50 mVs^{-1}

shell nanostructures were formed with a certain amount of Ag_2Al. After calcination at 873 K in air, the amorphous TiO_2 in the nanoporous Ag had not yet crystallized (Fig. 4), indicating that it possess a higher crystallization temperature. While, it has been found that the TiO_2 film in the calcined samples dealloyed at 333 K was partially crystallized (Fig. 6). Basing on the above analyses, we can draw a conclusion that the decomposition of Al-Ti and Ag_2Al could be promoted by water bath heating during the dealloying of Al-Ag-Ti alloys in NaOH solution, which was beneficial to the formation of the crystalline TiO_2 film. According to the previous work [23], the residual Al exists only in the form of Ag/Al compound. Furthermore, the thermal stability of nanoporous $Ag@TiO_2$ composites was found to be increased to 873 K due to the diffusion restraint of interfaces between Ag ligaments and TiO_2 shells [19].

Figure 8 shows the typical CV curves of 20 mM $NaBH_4$ in a 0.5 M KOH solution on the nanoporous Ag and $Ag@TiO_2$ electrodes at a scan rate of 50 mVs^{-1}. The electrodes were prepared by dealloying the $Al_{80-X}Ag_{20}Ti_X$ (X=0, 0.5, 1, 2, 3) ribbons in a 20 wt.% NaOH solution at 333 K for 30 h. The dealloyed samples were calcined at 873 K in air for 1 h. There were strong oxidation peaks at about −0.27 V in the CV curves of the nanoporous Ag electrode, which corresponds to the

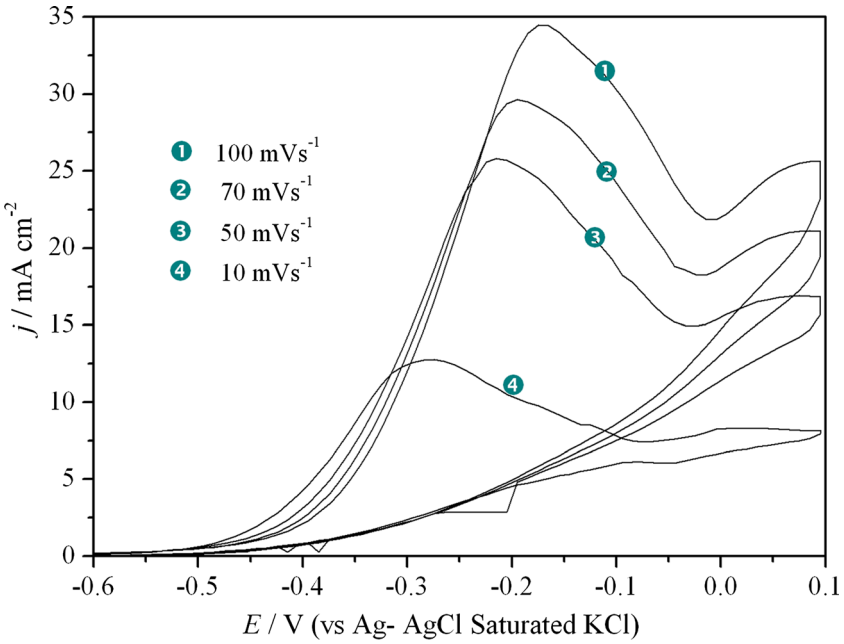

Fig. 9 CV curves of 20 mM $NaBH_4$ in a 0.5 M KOH solution on the nanoporous Ag/TiO_2 electrodes prepared by dealloying the $Al_{79}Ag_{20}Ti_1$ alloy at different scan rates

typical oxidation of BH_4^- on Ag nanoparticles [32, 33]. While, the current density of oxidation peak for the nanoporous Ag@TiO_2 electrode prepared from the $Al_{79.5}Ag_{20}Ti_{0.5}$ alloy increased from 10.91 to 18.13 mA cm^{-2}. With the increase of Ti content from 0.5 to 1.0 % in the precursor alloys, the current density of oxidation peak was observably increased to 28.86 mA cm^{-2}. With the further increase of Ti content, however, the current density of the nanoporous Ag@TiO_2 electrode was obviously decreased, and the position of oxidation peak became more positive. Especially, the electrode from the $Al_{77}Ag_{20}Ti_3$ alloy exhibited a very low current density. On the other hand, the BET surface areas of the composites prepared from the $Al_{79.5}Ag_{20}Ti_{0.5}$, $Al_{78}Ag_{20}Ti_2$, and $Al_{77}Ag_{20}Ti_3$ alloys were 6.61, 14.72, and 8.60 m^2/g. The results demonstrated that the content of Ti in the Al-Ag-Ti precursory alloys had an important influence on the formation of nanoporous structure, and a suitable amount of TiO_2 in the composites significantly enhanced the electrochemical activity toward the direct oxidation of sodium borohydride.

Figure 9 shows the effect of scan rates on the electrooxidation of $NaBH_4$ at the nanoporous Ag/TiO_2 electrode. It can be seen that the current density of the oxidation peak was significantly increased with the rise of the scan rate from 50 to 100 mVs^{-1}. At slow scan rate, the start of reaction at lower potentials confirmed that no self-inhibition occurs. The anodic peaks were shifted to more positive potentials due to the hydrolysis of BH^{4-} and the hydrogen ionization [34].

It is demonstrated that Ag/TiO_2 composites could exhibit the enhanced optical and catalytic properties owing to the electron transfer between Ag and TiO_2 [35]. The work function of Ag is lower than that of TiO_2; electrons can be removed from TiO_2 with high Fermi level to Ag through interface, resulting in the formation of Schottky barrier. While, the Schottky barrier can promote effectively electrons transfer from TiO_2 film to Ag [36, 37]. Therefore, the nanoporous Ag@TiO_2 composites exhibited an enhanced electrochemical performance for the oxidation of sodium borohydride. On the other hand, the high catalytic activity was also attributed to the formation of Ag^+ and Ti^{3+}. The Ag^+ species could act as the catalytic active sites for the oxidation reaction [38], and the Ti^{3+} increased the hydrophilicity of the nanoporous composites [39]. As a result, the prepared nanoporous Ag@TiO_2 composites exhibited an enhanced catalytic activity toward the direct borohydride oxidation due to their strong interfacial interactions (Fig. 8). However, with the increase of Ti content from 1 to 3 % in precursory alloys, charge transfer became much harder from TiO_2 film to Ag core, which caused a declining trend in catalytic activity (Fig. 8).

Conclusions

In summary, Nanoporous Ag@TiO_2 composites with core-shell structure were one-step prepared by dealloying the melt-spun Al-Ag-Ti alloys in NaOH aqueous solution. The surfaces of Ag ligaments in the nanoporous were covered by TiO_2 film with thickness of less than 4 nm. The decomposition of Ag_2Al and Ti-Al compounds in the Al-Ag-Ti alloys was promoted by water bath heating (333 K), resulting in the formation of nanoporous structure with high porosity. The Ag^+ and Ti^{3+} species could be generated in the composites by calcination, which were responsible for the enhanced catalytic activity. The electrochemical test results verify that the nanoporous Ag@TiO_2 composites as anode electrocatalyst drastically enhanced the direct oxidation of borohydride. The electrode prepared from the $Al_{79}Ag_{20}Ti_1$ alloy exhibited the highest peak current density, which increased from 10.91 to 28.86 mA cm^{-2}. The enhanced catalytic activity was attributed to the interfacial interactions between Ag cores and TiO_2 shells in the nanoporous structure. Furthermore, this approach could be extended to other nanoporous metal-TiO_2 composites, such as nanoporous Au@TiO_2 and Ag-Au@TiO_2.

Acknowledgments This work was financially supported by the National Natural Science Foundation of China (Grant No. 51371135, 11272223) and National Science and Technology Support Project of the Ministry of Science and Technology of China (Grant No. 2012BAE06B08).

References

1. Ding Y, Chen M (2009) MRS Bull 34:569–576
2. Senior NA, Newman RC (2006) Nanotechnology 17:2311–2316
3. Jia F, Yu C, Deng K, Zhang L (2007) J Phys Chem C 111:8424–8431
4. Li Q, Cui S, Yan X (2012) J Solid State Electrochem 16:1099–1104
5. Song TT, Gao YL, Zhang ZH, Zhai QJ (2013) Corros Sci 68:256–262
6. Wittstock A, Zielasek V, Biener J, Friend CM, Bäumer M (2010) Science 327:319–321
7. Xu C, Xu X, Su J, Ding Y (2007) J Catal 252:243–248
8. Erlebacher J, Aziz MJ, Karma A, Dimitrov N, Sieradzki K (2001) Nature 410:450–453
9. Luo X, Li R, Huang L, Zhang T (2013) Corros Sci 67:100–108
10. Mao R, Liang S, Wang X, Yang Q, Han B (2012) Corros Sci 60:231–237
11. Jia C, Yin H, Ma H, Wang R, Ge X, Zhou A, Xu X, Ding Y (2009) J Phys Chem C 113:16138–16143
12. Wittstock A, Wichmann A, Biener J, Bäumer M (2011) Faraday Discuss 152:87–98
13. Biener MM, Biener J, Wichmann A, Wittstock A, Baumann TF, Bäumer M, Hamza AV (2011) Nano Lett 11:3085–3090
14. Lang X, Hirata A, Fujita T, Chen M (2011) Nat Nanotechnol 6:232–236
15. Wittstock A, Wichmann A, Bäumer M (2012) ACS Catal 2:2199–2215
16. Su L, Gan YX (2012) Nano Energy 1:159–163
17. Wang X, Qi Z, Zhao C, Wang W, Zhang Z (2009) J Phys Chem C 113:13139–13150
18. Ji H, Wang X, Zhao C, Zhang C, Xu J, Zhang Z (2011) CrystEngComm 13:2617–2628
19. Ramasamy P, Seo DM, Kim SH, Kim J (2012) J Mater Chem 22:11651–11657
20. Feng C, Xu G, Liu H, Lv J, Zheng Z, Wu Y (2014) J Solid State Electrochem 18:163–171

21. Du P, Cao Y, Li D, Liu Z, Kong X, Sun Z (2013) RSC Adv 3:6016–6021
22. Pisarek M, Holdynski M, Roguska A, Kudelski A, Janik-Czachor M (2014) J Solid State Electrochem 18:3099–3109
23. Li GJ, Lu FF, Wei X, Song XP, Sun ZB, Yang ZM, Yang SC (2013) J Mater Chem A 1:4974–4981
24. Li G, Zhang X, Wang L, Song X, Sun Z (2013) J Electrochem Soc 160:F1116–F1122
25. Bera P, Patil KC, Hegde MS (2000) Phys Chem Chem Phys 2:3715–33719
26. Arabatzis IM, Stergiopoulos T, Bernard MC, Labou D, Neophytides SG, Falaras P (2003) Appl Catal B Environ 42:187–201
27. Liu C, Yang D, Jiao Y, Tian Y, Wang Y, Jiang Z (2013) ACS Appl Mater Interfaces 5:3824–3832
28. Linsebigler A, Rusu C, Yates JT (1996) J Am Chem Soc 118:5284–5289
29. Song T, Gao Y, Zhang Z, Zhai Q (2011) CrystEngComm 13:7058–7067
30. Zhang Q, Zhang Z (2010) Phys Chem Chem Phys 12:1453–1472
31. Hossein-Babaei F, Rahbarpour S (2011) Solid State Electron 56:185–190
32. Atwan MH, Northwood DO, Gyenge EL (2007) Int J Hydrogen Energy 32:3116–3125
33. Concha BM, Chatenet M (2009) Electrochim Acta 54:6130–6139
34. Martins JI, Nunes MC, Koch R, Martins L, Bazzaoui M (2007) Electrochim Acta 52:6443–6449
35. Du J, Zhang J, Liu Z, Han B, Jiang T, Huang Y (2006) Langmuir 22:1307–1312
36. Rao KVS, Lavedrine B, Boule P (2003) J Photochem Photobiol A 154:189–193
37. Sen S, Mahanty S, Roy S, Heintz O, Bourgeois S, Chaumont D (2005) Thin Solid Films 474:245–249
38. Feng RX, Dong H, Cao YL, Ai XP, Yang HX (2007) Int J Hydrogen Energy 32:4544–4549
39. Meng F, Sun Z (2009) Appl Surf Sci 255:6715–6720